THE JOURNAL OF BIOLOGICAL CHEMISTRY VOL. 281, NO. 45, pp. 34640–34650, November 10, 2006

Involvement of the Conserved Adaptor Protein Alix in Actin Cytoskeleton Assembly*[S]

Received for publication, March 10, 2006, and in revised form, July 10, 2006 Published, JBC Papers in Press, September 10, 2006, DOI 10.1074/jbc.M602263200

Shujuan Pan[‡1], Ruoning Wang[‡1], Xi Zhou[‡], Guangan He[‡], John Koomen[§], Ryuji Kobayashi[§], Le Sun[¶], Joe Corvera[¶], Gary E. Gallick[‖], and Jian Kuang[‡2]

From the Departments of [‡]Experimental Therapeutics, [§]Molecular Pathology, and [‖]Cancer Biology, the University of Texas, M. D. Anderson Cancer Center, Houston, Texas 77030 and [¶]A & G Pharmaceuticals, Inc., Baltimore, Maryland 21202

The conserved adaptor protein Alix, also called AIP1 or Hp95, promotes flattening and alignment of cultured mammalian fibroblasts; however, the mechanism by which Alix regulates fibroblast morphology is not understood. Here we demonstrate that Alix in WI38 cells, which require Alix expression for maintaining typical fibroblast morphology, associates with filamentous actin (F-actin) and F-actin-based structures lamellipodia and stress fibers. Reducing Alix expression by small interfering RNA (siRNA) decreases F-actin content and inhibits stress fiber assembly. In cell-free systems, Alix directly interacts with F-actin at both the N-terminal Bro1 domain and the C-terminal proline-rich domain. In Alix immunoprecipitates from WI38 cell lysates, actin is the most abundant partner protein of Alix. In addition, the N-terminal half of the middle region of Alix binds cortactin, an activator of the ARP2/3 complex-mediated initiation of actin polymerization. Alix is required for lamellipodial localization of cortactin. The C-terminal half of the middle region of Alix interacts with α-actinin, a key factor that bundles F-actin in stress fibers. Alix knockdown decreases the amount of α-actinin that associates with F-actin. These findings establish crucial involvement of Alix in actin cytoskeleton assembly.

Normal fibroblasts grow as a single layer, assume flattened and elongated cell shape, and align in parallel in monolayer culture. These morphological properties are determined by coordinated actin cytoskeleton assembly, integrin-mediated cell adhesion, and extracellular matrix assembly (1). Filamentous actin (F-actin)[3]-based structures, such as lamellipodia and filopodia at the leading edge of the cell and actin bundles in the central and peripheral regions of the cell body, are assembled adjacent to the plasma membrane and anchored to extracellular matrix through integrin-mediated cell adhesions (2–5). Dysregulation of any of these processes may cause alterations in fibroblast morphology, as often observed in transformed fibroblasts (6–8). Critical regulators of these processes are often identified by their ability to alter fibroblast morphology when their expression levels are increased or decreased.

Alix/AIP1 (ALG-2 interacting protein X or 1) is the mammalian ortholog of an evolutionally conserved family of adaptor proteins (9). Our investigation of biological functions of human Alix, which was originally identified by us and named Hp95 (10, 11), has revealed its critical roles in regulating fibroblast morphology. In immortalized mouse fibroblast NIH/3T3 cells that are less flattened and aligned than their nonimmortalized counterparts, overexpression of Alix promoted cell flattening and alignment, whereas reduction of Alix expression produced opposite effects (10). Alix overexpression also promoted cell flattening and monolayer growth in malignant HeLa cells (11). Because cell morphology is determined by coordinated actin cytoskeleton assembly, integrin-mediated cell adhesions, and extracellular matrix assembly, these findings indicate that Alix plays structural or regulatory roles in some of these processes.

Functional studies of Alix and its orthologs have generated the consensus that Alix is positively involved in apoptotic induction (9, 10, 12, 13) and sorting of endocytosed cell surface receptors into luminal vesicle of multivesicular bodies, also called late endosomes (14–16). Structurally, Alix and its orthologs are characterized by an N-terminal Bro1 domain, a middle region, and a C-terminal proline-rich domain (PRD). The Bro1 domain, named after the first identified ortholog of this family, yeast Bro1, was originally predicted by computer program-based sequence analysis and thought to consist of the N-terminal 160 amino acid residues. Recent x-ray crystallography of bacterially produced fragments of Bro1 suggested that the N-terminal 380 residues (called broad Bro1 domain) are required to form a structurally stable domain for partner protein interaction (17). The middle region contains coiled-coil motif, potential sites for additional partner protein interaction (15). The PRD contains multiple polyproline motifs, which are potential docking sites for proteins containing SH3 domains. The apoptotic function of Alix requires its interaction with the calcium-binding protein ALG-2 at the PRD (12, 18–20). The role of Alix in endosomal sorting requires binding the ESCRT-III component CHMP4b at the broad Bro1 domain and the ESCRT-I component TSG101 at the PRD (21–23). These functions of Alix do not seem to link to the effect of Alix on fibro-

* This work was supported by American Cancer Society Grant RPG-00-071-01-DDC and NCI Grant 1 RO1 CA93941 from the National Institutes of Health (to J. K.). The costs of publication of this article were defrayed in part by the payment of page charges. This article must therefore be hereby marked "*advertisement*" in accordance with 18 U.S.C. Section 1734 solely to indicate this fact.

[S] The on-line version of this article (available at http://www.jbc.org) contains supplemental Table S1 and Figs. S1–S4.

[1] Both authors should be considered as first authors.

[2] To whom correspondence should be addressed: Dept. of Experimental Therapeutics, the University of Texas M. D. Anderson Cancer Center, 1515 Holcombe Blvd., Box 019, Houston, TX 77030. Tel.: 713-792-8505; Fax: 713-792-3754; E-mail: jkuang@mdanderson.org.

[3] The abbreviations used are: F-actin, filamentous actin; siRNA, small interfering RNA; PRD, proline-rich domain; GST, glutathione *S*-transferase; GFP, green fluorescent protein; DTT, dithiothreitol; PBS, phosphate-buffered saline; TRITC, tetramethylrhodamine isothiocyanate; PMSF, phenylmethylsulfonyl fluoride; PIPES, 1,4-piperazinediethanesulfonic acid.

blast morphology. Besides these well established functions of Alix, Alix coimmunoprecipitated with epidermal growth factor receptor, multiple cytoskeletal proteins, including actin and focal adhesion kinases in crude lysates of rat astrocytes (24). Although the physical nature or the functional implication of these associations was not determined in this study, these observations raised the possibility that Alix is a component of the transmembrane protein network that orchestrate coordinated actin cytoskeleton assembly, integrin-mediated cell adhesions, and extracellular matrix assembly. To explore this possibility, we used nonimmortalized WI38 cells derived from human lung fibroblasts as the model system to determine where in the transmembrane protein network Alix performs functions that regulate cell morphology. Here we report that Alix associates with actin cytoskeleton and promotes its assembly.

EXPERIMENTAL PROCEDURES

Production of Recombinant Proteins—cDNAs that encode full-length and truncated Alix were generated by PCR using the Alix cDNA clone obtained in our previous studies as the template (11). PCR primers for full-length and truncated Alix are listed in supplemental Table S1. PCR products were digested with BamHI and NotI restriction enzymes and inserted into the BamHI and NotI sites of the pGEX-4T3 vector (Amersham Biosciences). To express recombinant proteins from these cDNAs, BL-21 *Escherichia coli* cells were transformed with produced cDNA constructs and induced at ~0.6 of A_{600} with 0.1 mM isopropyl 1-thio-β-D-galactopyranoside at 37 °C for 4 h. The induced cells were harvested by centrifugation at 5000 × *g* for 10 min and resuspended in phosphate-buffered saline (PBS) supplemented with 0.5% Triton X-100, 1 mM EDTA, 1 mM DTT, 0.35 M NaCl, 1 mM PMSF, 200 μg/ml lysozyme, 5 mM benzamidine (Sigma), and 1 μg/ml each of leupeptin, pepstatin A, and chymostatin (Roche Applied Science). The cells were then lysed by sonication, and the cell lysates were cleared by centrifugation at 13,000 × *g* for 40 min. To purify the recombinant proteins, the cleared cell lysates were incubated with glutathione-agarose (Sigma) overnight at 4 °C on rotation. The resins were then column-washed with 20-bed volumes of 500 mM NaCl, 0.1 mM EDTA, 0.1 mM EGTA, 0.5% Triton X-100, 0.5% Tween 20, and 1 mM DTT in 50 mM Tris-HCl (pH 8.0). Following the wash, recombinant proteins on the beads were eluted with 10 mM reduced glutathione in PBS and stored in 20% glycerol at −70 °C. To produce GST-tagged Alix or Alix fragments by *in vitro* transcription and translation, cDNAs encoding these recombinant proteins were amplified from their bacterial expression vectors by PCR with the forward primer 5′-atttaggtgacactatagaagcgag-ccaccatggcccctatactaggttattg-3′ and the reverse primer 5′-ccgggagctgcatgtgtcagaggttttc-3′. These PCR products were transcribed directly using mMESSAGE mMACHINE™ SP6 kit (Ambion, Austin, TX). Proteins were produced from the RNA products by *in vitro* translation using reticulocyte lysates by *in vitro* translation kit (Ambion, Austin, TX).

Production and Characterization of Anti-Alix Monoclonal Antibodies—Balb/c mice were immunized with purified GST-Alix. Two weeks after immunization, blood samples were obtained from the tail of the immunized mice and tested for titers against GST-Alix by both enzyme-linked immunosorbent assay and immunoblotting. Spleens from the mice that showed the highest titers were removed, and their splenocytes were fused with the mouse myeloma cell line SP2/0. Culture supernatants from individual hybridoma clones were then screened by enzyme-linked immunosorbent assay and immunoblotting against GST-Alix. To produce antibodies from different hybridoma clones, the clones were seeded in stationary bioreactors in Dulbecco's modified Eagle's medium (Invitrogen) plus 10% low IgG fetal bovine serum from HyClone (Logan, UT). The bioreactor fluids were collected every 3 days, and IgG fractions were affinity-purified using protein G-agarose columns (Upstate Biotechnology, Lake Placid, NY). The concentrations of purified IgG were determined by their absorbance at A_{280}.

Cell Culture and Transfection—WI38 cells, derived from human lung fibroblasts, were obtained from ATCC and cultured in regular culture dishes in Eagle's minimal essential medium with Earle's salts (Invitrogen) that was supplemented with 2 mM L-glutamine and 10% fetal bovine serum (Atlanta Biologicals, Lawrenceville, GA) unless otherwise indicated. WI38 cells were not immortalized, and the 19th to 30th generations were used in this study. Two Alix-specific siRNAs and one green fluorescence protein (GFP)-specific siRNA were designed and synthesized by Dharmacon Research Inc. (Lafayette, CO). Alix-specific siRNA sequences were 5′-gagaagaaau-ugcaagguu-3′ and 5′-gaaggaugcuuucgauaaa-3′. The GFP-specific siRNA sequence was 5′-ggcuacguccaggagcgcacc-3′. Transfection of siRNA was performed essentially as described previously (25). In brief, 2.5 × 10^5 WI38 cells were plated in 35-mm culture dishes and grown for 24 h. Each plate of cells was then transfected with 4 μl of 50 nM siRNA mixed with Lipofectamine-2000 purchased from Invitrogen following the manufacturer's instruction. The transfected cells were either continuously cultured or subcultured at 24 h after the transfection at 10^4 cells per new dish. Cell morphologies were observed after 48 and 72 h by phase contrast microscopy, and digital images were taken at ×40 magnifications by Olympus IX81 microscope (Olympus America Inc. Melville, NY) using Metamorph software (Molecular Devices Corp., Sunnyvale, CA).

Preparation of Cell Lysates, Immunoprecipitation, and Immunoblotting—For testing the immunoblotting and immunoprecipitation efficiencies of anti-Alix antibodies, WI38 cells were scraped from culture dishes in ice-cold RIPA buffer (1% Nonidet P-40, 0.5% deoxycholate, 0.1% SDS, and 150 mM NaCl in 20 mM Tris-HCl (pH 7.4)) supplemented with 1 mM PMSF and 1 μg/ml each of leupeptin, pepstatin A, and chymostatin (Roche Applied Science) and incubated on ice for 30 min. For testing interactions between Alix and cortactin and α-actinin, WI38 cells were lysed by sonication in buffer containing 20 mM Tris-HCl, 150 mM NaCl, 5 mM EDTA, 1 mM PMSF, and 1 μg/ml each of leupeptin, pepstatin A, and chymostatin. Collected cell lysates were centrifuged at 10,000 × *g* for 30 min, and protein concentrations of supernatants were determined by using a DC

protein assay kit purchased from Bio-Rad. Immunoprecipitation of WI38 cell lysates was performed by incubation of 40 μl of crude cell lysates (~40 μg of total proteins) with 2 μg of specific antibody immobilized onto 10 μl of protein G-Sepharose (Amersham Biosciences). The beads were then washed six times with 500 μl of lysis buffer and were eluted by boiling in 5 bed volumes of SDS-PAGE sample buffer. The eluted proteins were resolved by 10% SDS-PAGE, transblotted onto nitrocellulose membrane, and immunoblotted following the procedure as we described previously (26). Polyclonal anti-actin antibodies were purchased from Sigma. Polyclonal anti-cortactin and anti-Myc antibodies and monoclonal anti-α-actinin and anti-CDK4 antibodies were purchased from Santa Cruz Biotechnology (Santa Cruz, CA).

Immunofluorescence Staining—WI38 cells were cultured on 22-mm glass coverslips placed in a 35-mm culture dish. In some experiments, the glass coverslips were pre-coated at 4 °C overnight with 20 μg/ml fibronectin (Sigma). After indicated time of culture, cells were fixed with 4% paraformaldehyde (Sigma), permeabilized with 0.5% Triton X-100 (Sigma), and blocked for 1 h with 10% horse serum (Invitrogen) in PBS. Fixed cells were first incubated for 1 h with 1 μg/ml anti-Alix antibody diluted in 5% horse serum in PBS, followed by three washes with PBS, 0.1% Nonidet P-40. Cells were then incubated for 1 h with fluorescein isothiocyanate-conjugated secondary antibody (Sigma) diluted 1:200 in 3% horse serum in PBS. After three washings, cells were mounted with anti-fade (Vector Laboratories, Burlingame, CA), and images were captured by the Zeiss Axioplan 2 imaging system (Carl Zeiss Microimaging Inc., Thornwood, NY) using Metamorph software (Molecular Devices Corp.). For co-staining with antibody and phalloidin, after the final wash, cells were incubated with 50 μg/ml phalloidin-TRITC (Sigma) in PBS for 30 min and rinsed in PBS before mounting. For immunofluorescence staining with two antibodies, a mixture of the two antibodies was used as the primary antibody. Fluorescein isothiocyanate-conjugated anti-mouse IgG and Texas Red-conjugated anti-rabbit IgG (Vector Laboratories) were used to detect monoclonal and polyclonal antibodies, respectively. For cytochalasin D treatment, WI38 cells were cultured on 22-mm glass coverslips for 24 h, and the medium was replaced by fresh medium containing 5 μM of cytochalasin D (Sigma). After 30 min of incubation at 37 °C, cells were washed three times with PBS. Cells were then fixed and stained with phalloidin-TRITC following the same procedure described above.

GST Pulldown Assays—5 μg of purified GST or GST-tagged Alix or truncated Alix recombinant proteins were absorbed onto 5 μl of glutathione-conjugated agarose beads (Sigma). The beads were then incubated at 4 °C for 6 h with WI38 cell lysates (prepared in lysis buffer composed of 20 mM Tris-HCl (pH 7.4), 150 mM NaCl, 5 mM EDTA, 1 mM PMSF, and 1 μg/ml each of leupeptin, pepstatin A, and chymostatin) containing ~50 μg of total proteins. The beads were washed eight times with the lysis buffer plus 0.5% Nonidet P-40 and eluted with 40 μl of SDS sample buffer. Eluted polypepetides were resolved by 10% SDS-PAGE, transblotted onto nitrocellulose membrane, and immunoblotted with anti-cortactin or anti-α-actinin antibodies. To test Alix binding to G-actin, GST or GST-Alix absorbed glutathione-agarose beads were incubated at 4 °C overnight with 5 μg of purified non-muscle actin (Cytoskeleton, Denver, CO) dissolved in 40 μl of G-buffer (5 mM Tris-HCl (pH 8.0), 0.2 mM $CaCl_2$). The beads were washed eight times with G-buffer plus 0.5% Nonidet P-40 and 1 mM DTT and eluted with 40 μl of SDS sample buffer. Eluted polypeptides were resolved in parallel with nonabsorbed actin by 10% SDS-PAGE, transblotted onto nitrocellulose membrane, and immunoblotted with anti-actin antibodies.

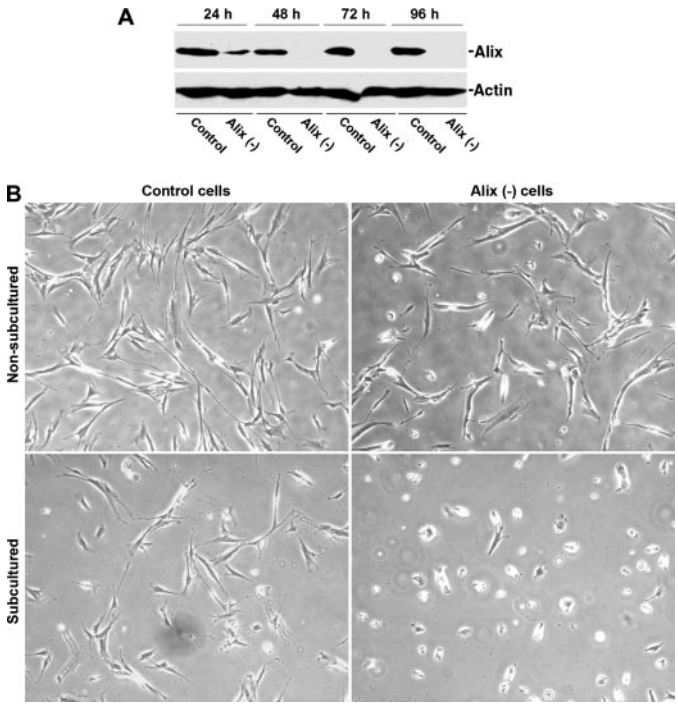

FIGURE 1. **Alix is required for WI38 cells to maintain typical fibroblast morphology.** *A,* immunoblots of Alix (*top panel*) and actin (*bottom panel*) in crude lysates of control or Alix siRNA-transfected WI38 cells collected at 24, 48, 72, and 96 h after the transfection. *B,* phase contrast images of control or Alix siRNA-transfected WI38 cells at 48 h after the transfection (*upper panel*) or that had been subcultured at 24 h after the transfection and further cultured for 24 h (*lower panel*).

F-actin Cosedimentation—F-actin cosedimentation assay was performed on Alix in WI38 cell lysates or GST-Alix recombinant proteins using the non-muscle actin-binding protein biochem kit specifically designed for this assay (Cytoskeleton). All the samples were pre-cleared by centrifugation at 150,000 × *g* for 1 h before the assay. Quantitation of Coomassie Blue-stained polypeptides in the supernatant and pellet was performed by analyzing scanned images with NIH Image 1.62 as described previously (10). Data were analyzed by the curve fitting software PRIZM when indicated (version 3; GraphPad Software, San Diego).

Separation of G-actin and F-actin in WI38 Cell Lysates—F-actin and G-actin in WI38 cell lysates was separated using a procedure described previously (27, 28). Briefly, WI38 cells were transfected with control or Alix siRNA. 48 h after transfection, cells were trypsinized, and 1×10^5 cells were re-plated into 35-mm dishes and cultured for an additional 3 h. Cells were then lysed in plate with 250 μl of actin stabilization buffer (0.1 M PIPES (pH 6.9), 30% glycerol, 5% Me_2SO, 1 mM $MgSO_4$, 2 μg/ml each of leupeptin, pepstatin A, and chymostatin) and incubated

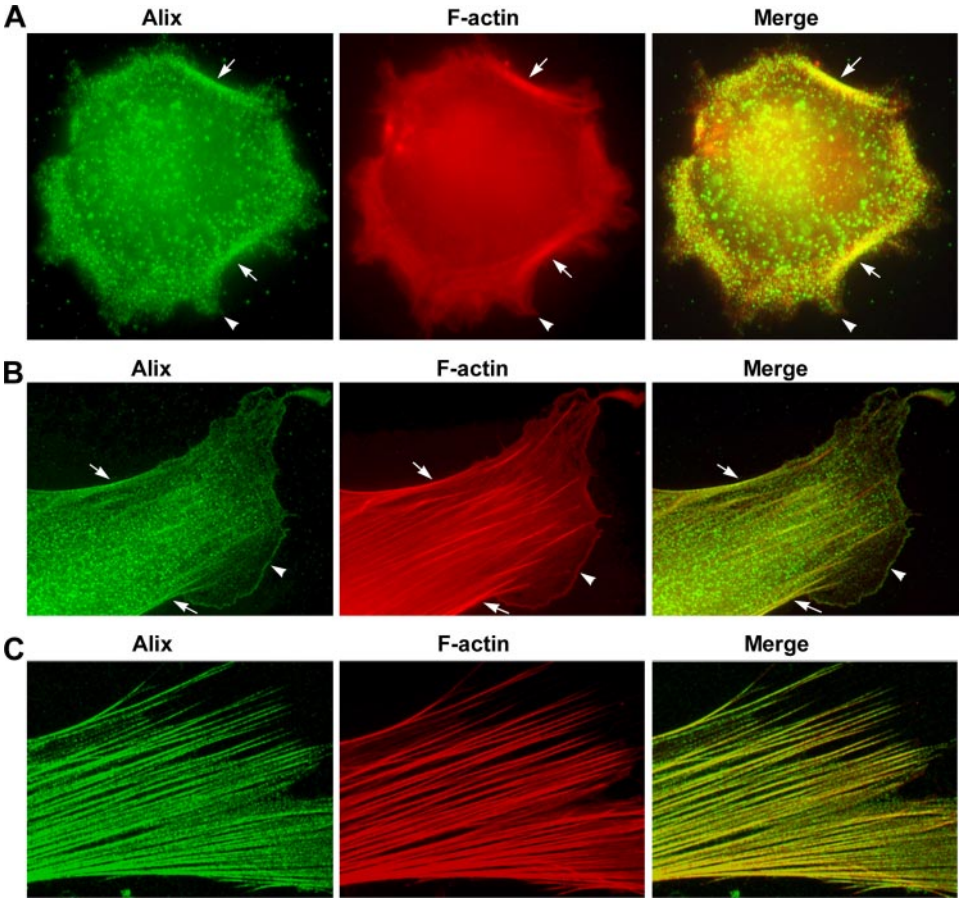

FIGURE 2. **Alix associates with actin cytoskeleton in WI38 cells.** WI38 cells that had been cultured for 1 (*A*) or 24 h (*B*) on nontreated glass coverslips or 24 h on glass coverslips pre-coated with fibronectin (*C*) were stained with 3A9 antibody for Alix (*green*) and phalloidin for F-actin (*red*). *Arrows* indicate association of Alix with stress fibers, and *arrowheads* indicate localization of Alix at lamellipodia or spreading lamella.

at 4 °C for 20 min. Lysed cells were scraped out of the plate and ultracentrifuged (100,000 × *g*) for 15 min at 4 °C in Beckman TLA100.1 ultracentrifuge rotor (Beckman Coulter, Fullerton, CA). The supernatant was collected and used as the G-actin fraction. The pellet was dissolved in 250 μl of lysis buffer supplemented with 5 μM cytochalasin D (Sigma) and used as the F-actin fraction. Equal percentages of the G-actin and F-actin fractions were resolved by SDS-PAGE and immunoblotted with antibodies that recognize actin, cortactin, or α-actinin.

Proteomic Analysis of Polypeptides in the Alix Complexes—5 μg of equally mixed 1A12, 1F7, 2H12, and 3A9 antibodies that were immobilized onto 40 μl of protein G-Sepharose were incubated with 2 ml of WI38 cell lysates containing ~2 mg of total proteins at 4 °C overnight and washed six times with RIPA buffer. The immunocomplexes were then eluted with 80 μl of SDS-PAGE sample buffer and resolved by 10% SDS-PAGE. After the gels were silver-stained, all visualized polypeptides that had been specifically precipitated by anti-Alix antibodies were excised and digested at 37 °C overnight with 100 ng of modified trypsin (Promega, Madison, WI). After extraction and vacuum concentration, samples were analyzed with LC-MS/MS on an electrospray ion trap mass spectrometer (LCQ DecaXP, Thermo, San Jose, CA). The following aqueous solvent system was used: solvent A contained 2% acetonitrile with 0.01% trifluoroacetic acid, and solvent B consisted of 20% 2-propanol, 60% acetonitrile, and 0.01% trifluoroacetic acid. The solvents were purchased from Burdick and Jackson (Muskegon, MI), and trifluoroacetic acid was acquired from Pierce. The gradient was ramped from 5% solvent B to 60% solvent B over 40 min using an Ultimate pump (Dionex, Sunnyvale, CA). Tandem mass spectra were subjected to data base searches using Mascot for trypsin and semi-trypsin enzyme specificities and allowing for methionine oxidation and as many as two missed cleavages.

RESULTS

Alix Is Required for WI38 Cells to Maintain Typical Fibroblast Morphology—Our previous investigation of the function of Alix in immortalized mouse fibroblast NIH/3T3 cells revealed roles of Alix in regulating fibroblast morphology. To determine whether this applies to the model system chosen for this study, we transfected WI38 cells with siRNA against either Alix or GFP (used as a negative control) and examined the effect of Alix knockdown on WI38 cell morphology. Immunoblotting of crude cell lysates with anti-Alix monoclonal antibodies generated by us showed that Alix expression decreased by 3–4-fold in Alix siRNA-transfected cells at 24 h and became hardly detectable at 48–96 h after the transfection, whereas actin expression did not decrease. In contrast to Alix siRNA-transfected cells, control transfected cells expressed constant levels of both Alix and actin (Fig. 1*A*). Parallel observation of the morphology of the transfected cells without a subculture revealed that Alix knockdown cells formed fewer membrane protrusions and looked blunter than control cells, although overall cell shapes were similar (Fig. 1*B*, *upper panel*). When control and Alix siRNA-transfected cells were first subcultured and then examined, the effect of Alix knockdown on cell morphology became more dramatic (Fig. 1*B*, *lower panel*) despite their comparable rates of cell growth and death (data not shown). These results indicated that Alix is required for WI38 cells to maintain typical fibroblast morphology.

Alix Associates with Actin Cytoskeleton in WI38 Cells—To investigate the role of Alix in the transmembrane network that regulates fibroblast morphology, we first determined the subcellular localization of Alix in WI38 cells in relation to F-actin-based structures with 1A12, 1F7, and 3A9 anti-Alix monoclonal antibodies and the F-actin-specific agent phalloidin (29, 30). These three antibodies were chosen because each efficiently

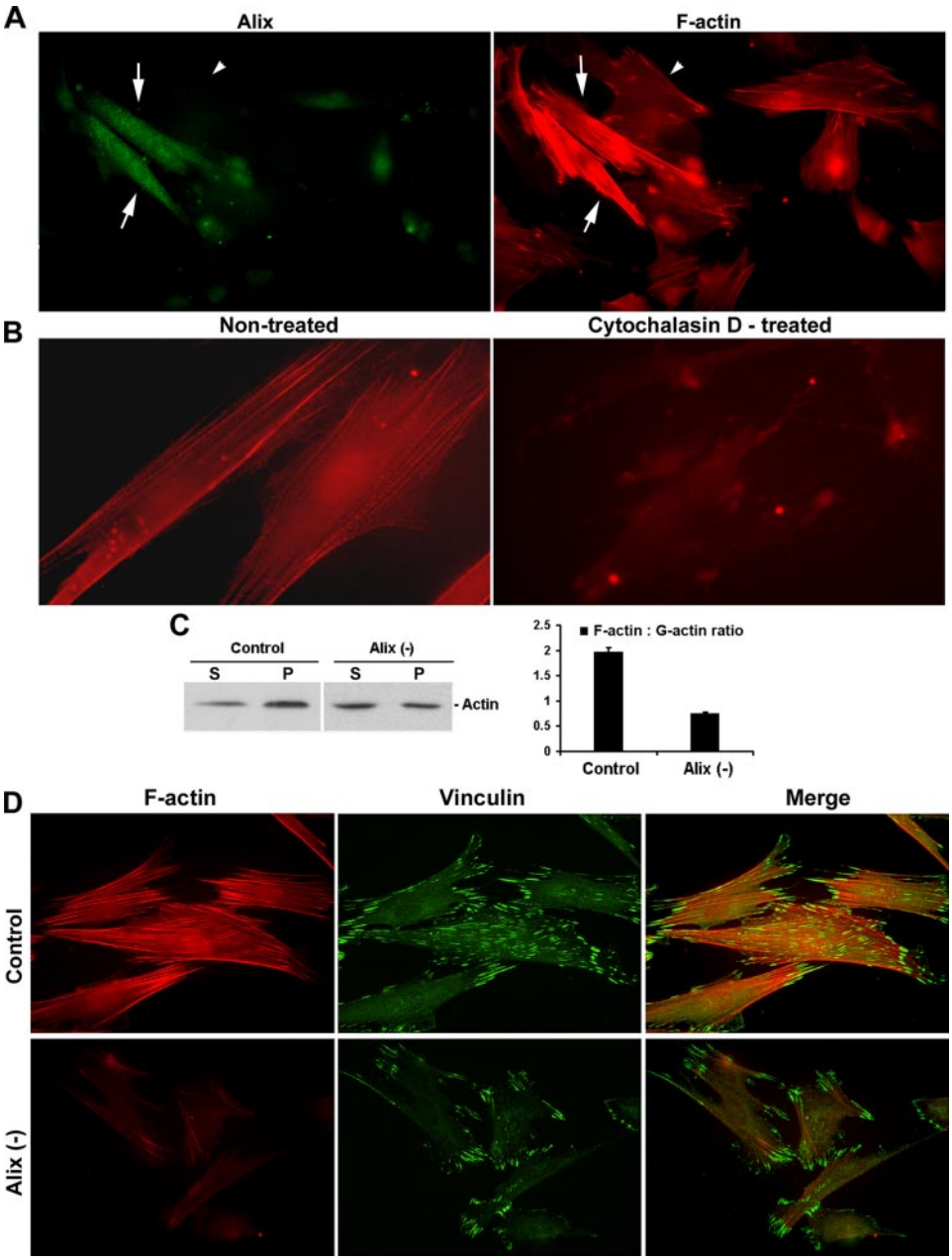

FIGURE 3. **Alix knockdown inhibits actin cytoskeleton assembly.** *A,* Alix siRNA-transfected cells were stained with 3A9 antibody for Alix (*green*) and phalloidin for F-actin (*red*). *Arrows* indicate the two cells in which Alix expression remained high, and *arrowheads* indicate adjacent Alix knockdown cells. *B,* phalloidin staining of F-actin in WI38 cells with or without pretreatment with 5 μM cytochalasin D. *C,* control or Alix knockdown WI38 cells were lysed in F-actin actin stabilization buffer and fractionated by ultracentrifugation. The proteins in the G-actin containing supernatant (*S*) and the F-actin containing pellet (*P*) were immunoblotted with anti-actin antibodies (*left panel*), and the F-actin to G-actin ratio in control and Alix knockdown cells was determined (*right panel*). *D,* control and Alix siRNA-transfected cells grown on fibronectin-coated substrata were double-stained with phalloidin for F-actin (*red*) and anti-vinculin antibodies for focal adhesions (*green*), and fluorescence images were taken under identical conditions.

immunoblotted and immunoprecipitated Alix in crude lysates of WI38 cells (supplemental Fig. S1). We observed that each of the three antibodies stained F-actin-based structures as well as free standing particles, which were probably endosomes based on previously established functions of Alix in endosomal sorting. In contrast, none of the antibodies stained structures at the cell periphery that assumed the shape of focal adhesions. As representatives, 3A9 antibody stained both protruding lamella at the cell edge and circumvential actin bundles at the base of the lamella in newly seeded cells that were spreading (Fig. 2*A*). In well spread cells, 3A9 antibody stained lamellipodia and stress fibers (Fig. 2*B*). When we cultured WI38 cells on fibronectin-coated substrata, which greatly enhanced stress fiber assembly, Alix almost quantitatively localized at stress fibers (Fig. 2*C*). These results demonstrated that Alix associates with actin cytoskeleton in WI38 cells.

Alix Knockdown Inhibits Actin Cytoskeleton Assembly in WI38 Cells—To determine whether Alix has functions in actin cytoskeleton assembly, we transfected WI38 cells with control or Alix-specific siRNA and stained cells with phalloidin, which stains both F-actin that has been assembled into high order structures and short F-actin scattered in the cytoplasm (31–34). Clearly, the F-actin staining was universally weaker in Alix knockdown cells than in control cells. The difference was best illustrated by concurrent staining of the majority of Alix siRNA-transfected cells and the few nontransfected cells in the same field (Fig. 3*A*). However, no change was observed in the protein level of actin (Fig. 1*A*). Treatment of WI38 cells with the F-actin depolymerization agent cytochalasin D reduced the overall staining by phalloidin as well (Fig. 3*B*). These results indicated that Alix knockdown inhibits F-actin formation in WI38 cells. In support of this conclusion, when crude lysates of control and Alix knockdown WI38 cells were fractionated into F-actin-containing and G-actin-containing fractions, the F-actin:G-actin ratio in control cells was ~3-fold higher than that in Alix knockdown cells (Fig. 3*C*).

In addition to the negative effect of Alix knockdown on the F-actin content, Alix knockdown cells also assembled less stress fibers than control cells, especially in central areas of the cell. This difference was most obvious when cells were grown on fibronectin-coated substrata, which enhances stress fiber assembly (Fig. 3*D*, *left panel*). In contrast, control and Alix knockdown cells formed comparable numbers of focal adhesions, as revealed by immunofluorescence staining of vinculin (Fig. 3*D*, *middle panel*), eliminating the possibility that Alix knockdown inhibits stress fiber assem-

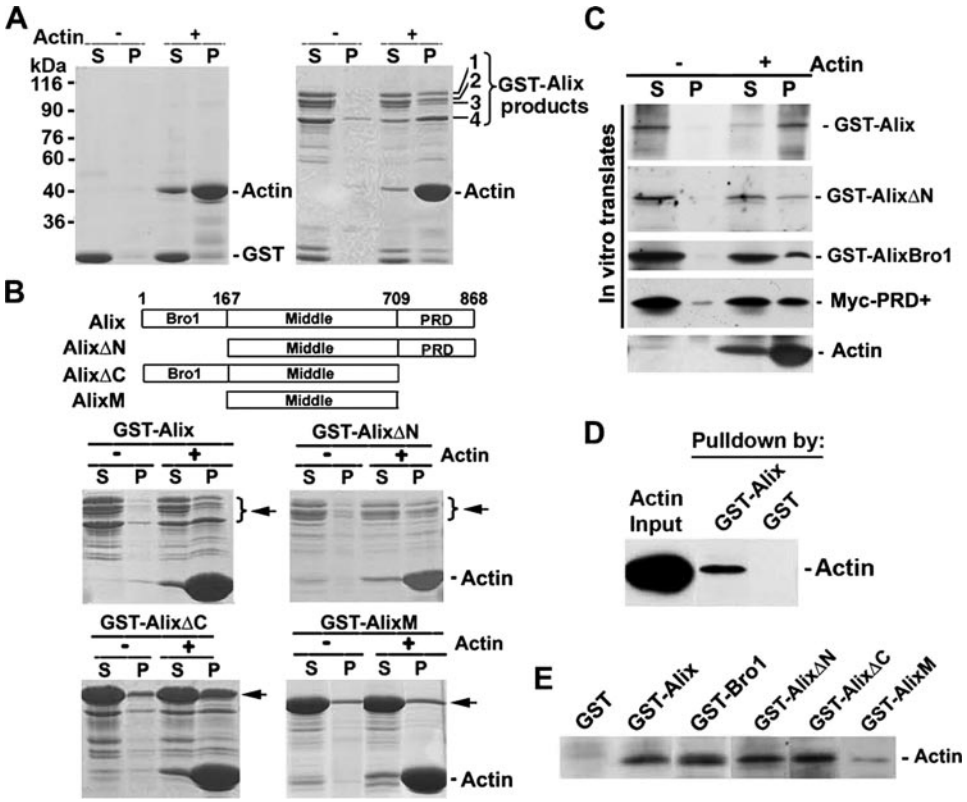

FIGURE 4. **Alix directly interacts with actin in cell-free systems.** *A,* Coomassie Blue staining of soluble (*lane S*) and pelleted (*lane P*) fractions of GST (*left panel*) or GST-Alix (*right panel*) after their incubation with actin-polymerization buffer (F-buffer) alone or the buffer containing 10 μg of actin and ultracentrifugation. The four major polypeptides of GST-Alix sample are indicated. Four major polypeptides in the GST-Alix samples are indicated. *B,* schematic illustration of the Alix portion of different GST-Alix fusion proteins and Coomassie Blue staining of soluble (*lane S*) and pelleted (*lane P*) fractions of each of these proteins after incubation with actin-polymerization buffer, or the buffer containing 10 μg of actin. *Arrows* indicate the major polypeptides in each of the GST-Alix fusion proteins. *C,* each of the indicated *in vitro* translates was incubated with actin-polymerization buffer (−), or the buffer containing 10 μg actin (+), and the soluble (*lane S*) and pelleted (*lane P*) fractions of the end products were immunoblotted for each of the indicated proteins. *D,* immunoblots of input actin or actin that was pulled down by immobilized GST or GST-Alix. *E,* immunoblots of actin that was pulled down by each of the indicated proteins.

bly in WI38 cells through inhibiting integrin-mediated cell adhesions.

Alix Directly Interacts with Actin—To characterize the mechanism by which Alix associates with actin cytoskeleton and promotes its assembly, we initially determined whether Alix directly interacts with actin. For this, we first induced polymerization of commercial G-actin in the presence of bacterially produced GST-Alix or GST alone and determined their interaction with F-actin by the F-actin cosedimentation assay (35). As shown in Fig. 4, 30–70% of the four major polypeptides in the GST-Alix sample co-pelleted with F-actin, whereas the negative control GST remained in the supernatant. Mass spectrometry analyses of these four polypeptides revealed that they contained residues 1–802, 1–759, 1–745, and 1–574 of Alix, respectively (supplemental Fig. S2). These results indicated that an N-terminal region of Alix directly interacts with F-actin. To further characterize the region in Alix that interacts with F-actin, we produced GST-tagged Alix truncation products that lacked the N-terminal Bro1 domain (GST-AlixΔN), the C-terminal Pro-rich domain (GST-AlixΔC), or both of them (GST-AlixM) in bacteria and examined their interaction with F-actin by the F-actin cosedimentation assay. Although GST-AlixΔN and GST-AlixΔC bound F-actin as efficiently as GST-Alix, GST-AlixM hardly bound F-actin (Fig. 4*B*). These results indicated that the N-terminal Bro1 domain and the C-terminal PRD of Alix may each contain a docking site for F-actin. To test this possibility, we next produced noncleaved GST-Alix, GST-AlixΔN, GST-Bro1, and Myc-tagged PRD plus the adjacent 100 residues of Alix (myc-PRD+) by *in vitro* translation and determined their interaction with F-actin by the cosedimentation assay. PRD+ was Myc-tagged because it had already been produced for a separate study. Approximately 30–70% of GST-Alix, GST-AlixΔN, GST-Bro1, or myc-PRD+ cosedimented with F-actin (Fig. 4*C*), confirming that both the Bro1 domain and the PRD interact with F-actin. Finally, to determine whether Alix interacts with G-actin as well, we incubated various GST-tagged Alix products from bacteria with commercial G-actin and examined G-actin retention by the GST pulldown assay. A small percentage of G-actin input (5–10%) was pulled down by GST-Alix but not GST alone (Fig. 4*D*). Although GST-Bro1, GST-AlixΔN, and GST-AlixΔC pulled down similar amounts of G-actin as did GST-Alix, GST-AlixM pulled down little G-actin (Fig. 4*E*). These results indicated that the Bro1 domain and the PRD of Alix interact with G-actin as well although probably at a much lower affinity than with F-actin.

Alix Interacts with F-actin in a Dose-dependent and Stoichiometric Manner—To obtain insights into the mode of Alix/F-actin interaction, we performed two series of F-actin polymerization reactions in the presence of bacterially produced GST-AlixΔC followed by ultracentrifugation. GST-AlixΔC was used in this experiment because it contained less cleavage products than GST-Alix and could be quantitated more accurately. The first series consisted of a fixed concentration of G-actin (1.2 μM) and variable concentrations of GST-AlixΔC (0.06–1.0 μM). Because we had determined that ~30% of GST-AlixΔC was available for F-actin binding (data not shown), actin was in excess at all GST-AlixΔC concentrations. As shown in Fig. 5*A*, the amount of GST-AlixΔC that bound to F-actin increased in parallel with the amount of the input GST-AlixΔC, indicating that Alix binds to F-actin in a dose-dependent manner. The second series of reactions consisted of variable concentrations of G-actin (0–8 μM) and a fixed concentration of GST-AlixΔC (1 μM). As shown in Fig. 5*B*, the amount of GST-AlixΔC that bound to F-actin reached a

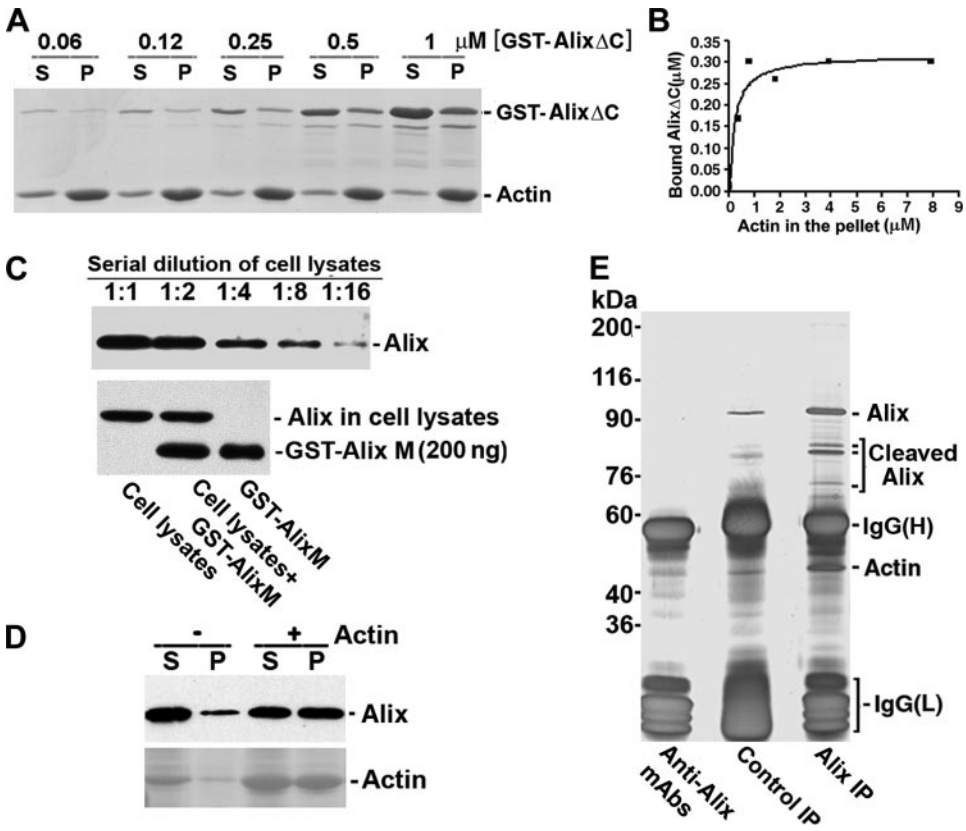

FIGURE 5. **Actin is a major partner protein of Alix in WI38 cells.** *A,* after indicated concentrations of GST-AlixΔC were incubated with actin-polymerization buffer containing 1 μM G-actin followed by ultracentrifugation, the soluble (*lane S*) and pelleted (*lane P*) fractions of the protein were separated by SDS-PAGE and stained by Coomassie Blue. *B,* 1 μM GST-AlixΔC was incubated with increased concentrations (0–8 μM) of G-actin in the actin-polymerization buffer followed by ultracentrifugation. After the proteins in the pellets and supernatants were resolved by SDS-PAGE and stained by Coomassie Blue, the molar amounts of pelleted GST-AlixΔC against molar amounts of pelleted F-actin were quantified by densitometry and plotted with PRIZM software. *C,* serially diluted WI38 cell lysates (*upper panel*) and either or both of 30 μg of protein lysates of WI38 cells and 200 ng of GST-AlixM (*bottom panel*) were immunoblotted with 1F7 antibody. *D,* WI38 cell lysates were incubated with actin-polymerization buffer or the buffer containing 10 μg of actin, and the soluble (*lane S*) and pelleted (*lane P*) fractions of the end products were immunoblotted for Alix and stained with Ponceau S for actin. *E,* silver staining of proteins in the immunoprecipitates of crude lysates of WI38 cells with anti-Alix antibodies or mouse IgG. The bands indicated by *dashes* were identified by mass spectrometry.

plateau at 1.2 μM actin, implying that actin was in excess at and above this actin concentration, whereas GST-AlixΔC was in excess below this actin concentration. Most importantly, at 0.6 μM actin, ~0.17 μM GST-AlixΔC co-pelleted with ~0.4 μM F-actin, indicating that on the average one molecule of GST-AlixΔC may bind two molecules of actin.

Alix Is an Abundant Protein—Because actin is an abundant protein, the dose-dependent and stoichiometric interaction of Alix with F-actin in cell-free systems raised the possibility that Alix is an abundant protein as well. To test this possibility, we immunoblotted 30 μg of total proteins from WI38 cells either together or in parallel with 200 ng of GST-tagged middle region of Alix (GST-AlixM) with 1F7 antibody and estimated the amount of Alix in the total cellular proteins. GST-AlixM was used as a standard because it was clearly separated from endogenous Alix by SDS-PAGE. 1F7 antibody was chosen because this antibody recognized GST-Alix and GST-AlixM at similar efficiencies (data not shown). To obtain a reference for quantifying immunoblot signals, serially diluted WI38 cell lysates were immunoblotted (Fig. 5*C*, *upper panel*). It was observed that 200 ng of GST-AlixM generated 3-fold higher signals than the Alix in the cellular proteins (Fig. 5*C*, *lower panel*). Taking the mass difference between GST-AlixM and Alix into consideration, we estimated that Alix accounts for 0.25% of the total proteins in WI38 cell lysates, placing Alix into the category of abundant F-actin-binding proteins.

Actin Is a Major Partner Protein of Alix—Alix has been reported to associate with a variety of partner proteins that regulate apoptosis, endosomal sorting, and endocytosis. To estimate the relative abundance of Alix in WI38 cell lysates that associates with F-actin, we induced actin polymerization in WI38 cell lysates for 30 min, centrifuged the end products to pellet polymerized actin, and then determined the percentage of Alix that cosedimented with F-actin. By immunoblotting, ~50% of Alix in WI38 cell lysates co-pelleted with polymerized actin (Fig. 5*D*), whereas little Cdk4 (used as a negative control) was recovered in the pellet fraction (data not shown). These results indicated that actin is a major partner protein of Alix in WI38 cells. To further examine this issue, we immunoprecipitated crude lysates of WI38 cells grown under regular culture conditions with a combination of multiple anti-Alix monoclonal antibodies and analyzed the immunocomplexes by silver staining and mass spectrometry. As shown in Fig. 5*E*, actin was the major non-IgG polypeptide detected in the Alix immunoprecipitate besides the full-length and cleaved Alix. In contrast, none of the previously identified Alix binding partners that should not be masked by the heavy and light chains of the precipitating antibodies were detected, which is indicative of their absence or low abundance in the Alix immunoprecipitate. Although the control precipitate contained actin as well, the level was much lower than in the Alix immunoprecipitate, and its presence could be eliminated by more thorough washing, which did not eliminate actin in the Alix immunoprecipitate (data not shown). The control immunoprecipitate also contained a protein that comigrated with Alix. However, mass spectrometric analysis of this protein disproved its being Alix. These results further indicated that actin is a major partner protein of Alix in WI38 cells.

Alix Interacts with Cortactin—Because Alix is an adaptor protein, its interaction with F-actin and localization at lamellipodia raised the possibility that Alix interacts with an F-actin-binding protein at lamellipodia. Cortactin is one of the major F-actin-binding proteins at lamellipodia where it promotes and

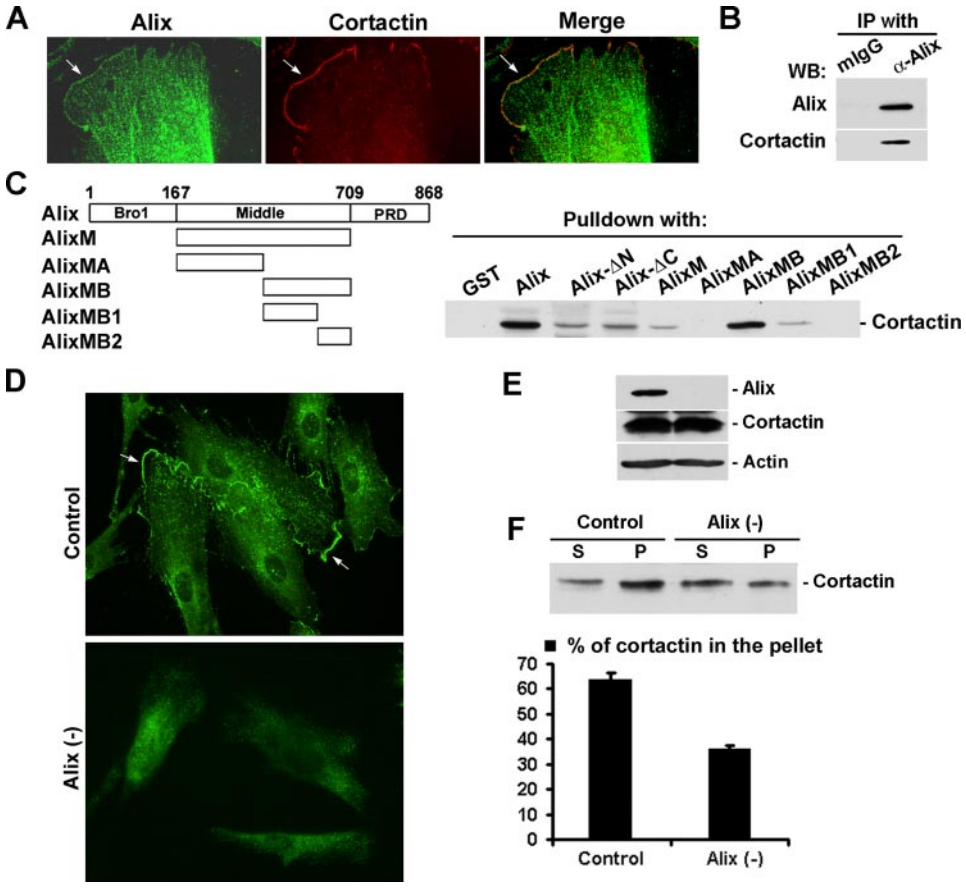

FIGURE 6. **Alix interacts with cortactin and promotes cortactin localization to the cell periphery.** *A,* WI38 cells were double-stained with 3A9 anti-Alix antibody (*green*) and anti-cortactin antibodies (*red*). *Arrows* indicate colocalization of Alix with cortactin at lamellipodia. *B,* WI38 cell lysates were immunoprecipitated (*IP*) with anti-Alix antibodies or mouse IgG (*mIgG*), and immunocomplexes were immunoblotted (*WB*) with anti-Alix or anti-cortactin antibodies. *C,* equal molars of the illustrated GST fusion proteins that were immobilized onto glutathione-Sepharose were incubated with WI38 cell lysates containing 100 μg of total proteins, and bound proteins were immunoblotted with anti-cortactin antibodies. *D,* control or Alix knockdown WI38 cells that had been cultured on fibronectin-coated substrata and in serum-free medium for 24 h were immunostained with anti-cortactin antibodies. *Arrows* indicate cortactin localization at lamellipodia. *E,* equal amounts of crude lysates of control and Alix knockdown WI38 cells were immunoblotted for each of the indicated proteins. *F,* control or Alix knockdown WI38 cells were lysed in the actin stabilization buffer and F-actin in crude cell lysates were pelleted by ultracentrifugation. Proteins in the supernatants (*lane S*) and pellets (*lane P*) were immunoblotted with anti-cortactin antibodies (*upper panel*). After relative amounts of cortactin in the paired samples were determined, the percentage of cortactin in the pellet fraction (*P*) was calculated for control and Alix knockdown cells, respectively.

stabilizes ARP2/3 complex-induced actin network formation (36, 37). Cabezas *et al.* (38) showed in a recent study that Alix knockdown in HeLa cells caused abnormal distribution of endosomes and the cortical actin cytoskeleton proteins such as cortactin and clathrin; therefore, we explored the possibility that Alix interacts with cortactin. For this objective, we first double-stained WI38 cells with anti-cortactin and anti-Alix antibodies. As shown in Fig. 6*A*, Alix staining colocalized with cortactin staining at lamellipodia. Second, we determined biochemical interaction of Alix with cortactin by coimmunoprecipitation and recombinant protein pulldown assays. After immunoprecipitation of WI38 cell lysates with anti-Alix antibodies or mouse IgG, cortactin was detected in the Alix immunoprecipitate but not in the control immunoprecipitate. Incubation of WI38 cell lysates with various Alix products followed by immunoblotting of the bound proteins with anti-cortactin antibodies showed that cortactin interacted with all of the Alix fragments that contained residues 436–609 (MB1) in the C-terminal half of the middle region (Fig. 6*C*), indicating that this non-actin binding region contains a cortactin-docking site. Third, we determined the effects of Alix knockdown and cytochalasin D treatment on cortactin localization by immunofluorescence microscopy. Both Alix knockdown and cytochalasin D treatment reduced phalloidin staining and inhibited stress fiber assembly as described earlier. However, whereas cytochalasin D treatment did not eliminate cortactin localization at the cell periphery (supplemental Fig. S4), Alix knockdown cells completely abolished it (Fig. 6*D*). This was in contrast to no change in the level of cortactin expression in Alix knockdown cells (Fig. 6*E*). Finally, we determined the effect of Alix knockdown on the relative abundance of cortactin in the G-actin and F-actin fractions by biochemical approaches; Alix knockdown reduced the percentage of cortactin in the F-actin fraction by 2-fold (Fig. 6*F*). Together, these results indicated that Alix directly interacts with cortactin and that this interaction plays important roles in localizing cortactin to lamellipodia.

Alix Interacts with α-Actinin—Alix association with stress fibers raised the possibility that Alix may interact with an F-actin-binding protein that preferentially localizes at stress fibers. To explore this possibility, we investigated Alix interaction with α-actinin, an F-actin-bundling protein that primarily associates with stress fibers (39). By immunoprecipitation of WI38 cell lysates with anti-Alix or anti-α-actinin antibodies followed by reciprocal immunoblotting, Alix and α-actinin interacted with each other in WI38 cell lysates (Fig. 7*A*). Mapping the α-actinin-binding region in Alix as we did for cortactin showed that it locates in the N-terminal portion of the middle region of Alix (residues 167–436, MA) (Fig. 7*B*), which bound neither F-actin (Fig. 4*B*) nor cortactin (Fig. 6*B*). Interestingly, the MA fragment consistently pulled down more α-actinin than the M fragment, suggesting that the MB fragment contains inhibitory sequences for Alix association with α-actinin. Next, we determined the effect of Alix knockdown on α-actinin association with F-actin and stress fibers. Although Alix knockdown did not affect α-actinin expression (Fig. 7*C*), Alix knockdown reduced the relative abundance of α-actinin in the F-actin fraction by 2-fold, as determined by immunoblotting of

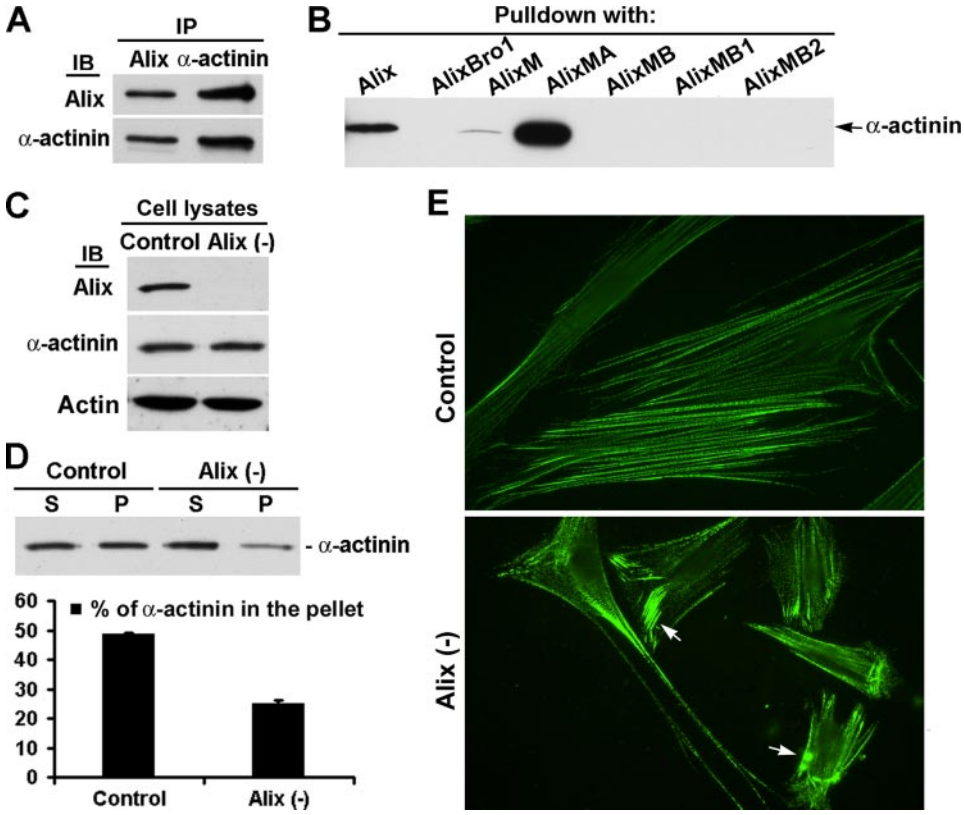

FIGURE 7. **Alix interacts with α-actinin and promotes α-actinin association with F-actin.** *A,* WI38 cell lysates were immunoprecipitated (*IP*) with 3A9 or anti-α-actinin antibodies, and the immunoprecipitates were immunoblotted (*IB*) for both Alix and α-actinin. *B,* WI38 cell lysates were incubated with GST or GST-Alix fusion proteins illustrated in Fig. 6*C*, and bound proteins were immunoblotted with anti-α-actinin antibodies. *C,* equal amounts of crude lysates of control and Alix knockdown WI38 cells were immunoblotted for each of the indicated proteins. *D,* control or Alix knockdown (−) WI38 cells were lysed in the actin stabilization buffer, and F-actin in crude cell lysates was pelleted by ultracentrifugation. Proteins in the supernatants (*lane S*) and pellets (*lane P*) were immunoblotted with anti-α-actinin antibodies (*upper panel*). After the relative amounts of α-actinin in the paired two fractions were determined, the percentage of α-actinin recovered in the pellet fraction (*P*) was calculated for control and Alix knockdown cells, respectively. *E,* control or Alix knockdown WI38 cells were immunostained with anti-α-actinin antibodies. *Arrows* indicate aggregates of α-actinin in Alix knockdown cells.

tent and inhibits F-actin assembly into higher order structures. In addition, recombinant Alix interacts with F-actin in a dose-dependent and stoichiometric manner in a cell-free system, and actin is the most abundant partner protein of Alix in WI38 cell lysates. Recombinant Alix also independently binds cortactin, which activates the ARP2/3 complex-mediated initiation of actin polymerization, and α-actinin, a key factor that bundles F-actin in stress fibers. Alix knockdown reduces the amount of cortactin and α-actinin in the F-actin fraction and abolishes lamellipodial localization of cortactin. These findings establish direct involvement of Alix in actin cytoskeleton assembly and uncovered at least one of the major mechanisms by which Alix regulates fibroblast morphology. Moreover, our findings offer a plausible explanation for the recent observation that Alix knockdown in HeLa cells caused an abnormal distribution of endosomes and the cortical proteins involved in endocytosis such as clathrin and cortactin (38).

Alix knockdown consistently reduces the overall cell staining by phalloidin, which stains both distinct F-actin-based structures such as lamellipodia and stress fibers and "amorphous" F-actin meshworks and scattered F-actin in the cytoplasm (31–34) (Fig. 3*B*). This indicates that Alix plays positive roles in actin polymerization or stability. Previous studies have established that actin polymerization is nucleated at lamellipodial protrusions or endosomes by membrane-associated Arp2/3 complex (40). Cortactin binds the Arp2/3 complex and activates the Arp2/3 complex-mediated actin polymerization. This process not only drives lamellipodial protrusions at the plasma membrane and directional movement of endosomes in the cytoplasm (37) but also determines the abundance of F-actin that can be assembled into stress fibers and other types of F-actin-based structures (41, 42). Based on these previous findings, the inhibitory effect of Alix knockdown on lamellipodial localization of cortactin may explain or contribute to the negative effects on both F-actin content.

In addition to reduced F-actin content, Alix knockdown cells also formed fewer and shorter stress fibers, especially in the central region of the cells (Fig. 3*D*). Although this abnormality can be simply attributed to the reducing effect of Alix knockdown on the F-actin content, Alix localization at stress fibers and Alix association with the F-actin bundling protein α-acti-

α-actinin in the G-actin and F-actin fractions in crude lysates of control and Alix-siRNA-transfected cells (Fig. 7*D*). Moreover, when control and Alix knockdown cells were grown on fibronectin-coated substrata stained with anti-α-actinin antibodies, α-actinin assumed a pattern of stress fibers in control cells, whereas it existed as clumps or thick bundles at the cell periphery in Alix knockdown cells (Fig. 7*E*). Together, these results indicated that Alix interacts with α-actinin and suggested that this interaction promotes α-actinin interaction with F-actin and its roles in stress fiber assembly.

DISCUSSION

We demonstrated previously that Alix promotes cell flattening and alignment in immortalized NIH/3T3 cells (10). This study made the first attempt to dissect the mechanism by which Alix regulates cell morphology. Using nontransformed WI38 cells as the model system, which requires Alix expression for maintenance of typical fibroblast morphology, we have discovered that Alix associates with both F-actin and the F-actin-based structures lamellipodia and stress fibers. Dramatically reducing Alix expression by siRNA both decreases F-actin con-

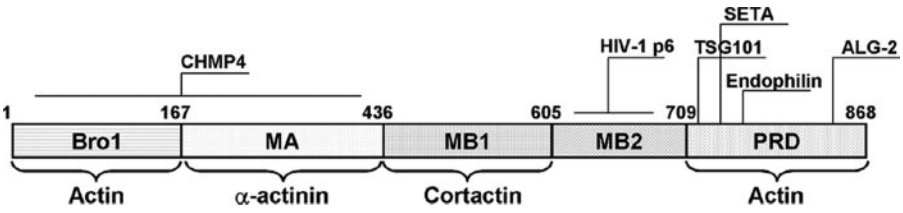

FIGURE 8. **Schematic illustration of conserved domains in Alix and regions in Alix that bind F-actin or F-actin-binding proteins.** The conserved domains of Alix and docking sites/regions for previously identified binding partners of Alix (on the *top*) and actin cytoskeleton proteins (at the *bottom*) are illustrated.

nin raise the possibility that Alix has an independent function in stress fiber assembly. Previous studies have established that key steps in stress fiber assembly are bundling of F-actin by α-actinin and association with F-actin bundles with myosin bundles (39). Because Alix directly interacts with α-actinin and promotes its association with F-actin, Alix may play a positive role in the F-actin bundling step in stress fiber assembly.

Alix has been implicated in diverse cellular processes by binding a variety of partner proteins. However, none of these previous studies examined the relative abundance of these proteins in the Alix complexes in any cell systems or provided quantitative information on partition of Alix to different structures or functions. In this study, we performed the first proteomic analysis of the components in the Alix complex in mammalian cells lysates and obtained evidence that actin is a major Alix binding partner in WI38 cells. This was consistent with colocalization of the majority of the Alix staining with F-actin staining in WI38 cells. These findings indicate that regulation of actin cytoskeleton assembly is a major biological function of Alix in mammalian fibroblasts.

The yeast ortholog of Alix, Bro1, was originally identified by mutations causing increased osmotic sensitivity. In addition to this defect, the mutant cells showed larger sizes and abnormal cell shapes (43). However, neither the characterized roles of Bro1 in endosomal trafficking nor other known functions of Bro1 or related proteins account for these morphological defects. Because proper assembly of cortical cytoskeleton by F-actin cross-linking proteins has been demonstrated to protect yeast cells from osmotic stress and ensure normal cell sizes and shapes (44), it is conceivable that the role of Alix in regulating the actin cytoskeleton is evolutionally conserved and that Bro1 mutation generates these mutant phenotypes through causing defects in the actin cytoskeleton.

Alix is structurally characterized by an N-terminal Bro1 domain, a middle region, and a C-terminal PRD (14). As illustrated in Fig. 8, previous studies have established that the PRD interacts with multiple cellular Alix-binding partners that are involved in apoptotic induction (ALG-2), endosomal sorting (TSG-101), and endocytosis (SETA/CIN85) (20, 21, 23, 45). A short region adjacent to the PRD interacts with two viral proteins (P6 and P9) (21). Moreover, the recently defined broad Bro1 domain, which includes both the Bro1 domain and the C-terminal 200 residues, interacts with CHMP4b also involved in endosomal sorting (17). In this study, we have demonstrated that both the Bro1 domain and the PRD bind F-actin. This is the first example that the structurally conserved Bro1 domain actually interacts with a partner protein. The N-terminal half of the middle region of Alix interacts with α-actinin. The C-terminal half of the middle region of Alix contains a docking site for cortactin, which localizes before the region that interacts with the two viral proteins. The involvement of all major regions of Alix in its interaction with actin cytoskeleton proteins predicts that the role of Alix in actin cytoskeleton assembly involves the whole molecule and that a truncated Alix may have dominant negative effects on the role of Alix in actin cytoskeleton assembly. Consistent with this possibility, the Alix-related protein rhophilin, which contains an intact Bro1 domain but lacks a counterpart of the middle region or the PRD of Alix (46, 47), was previously shown to inhibit stress fiber assembly in a Bro1 domain-dependent manner (47).

Acknowledgments—The electron microscopy work was performed with the help of the High Resolution Electron Microscopy Facility at the University of Texas M. D. Anderson Cancer Center, which was funded by Institutional Core Grant CA16672. We thank Drs. W. N. Hittelman, J. Izzo, and L. Tao for instructions in using the Zeiss Axioplan 2 imaging system. We thank Dr. R. B. Clark and J. Friedman for critically reading the manuscript.

REFERENCES

1. Geiger, B., Bershadsky, A., Pankov, R., and Yamada, K. M. (2001) *Nat. Rev. Mol. Cell Biol.* **2,** 793–805
2. Mitchison, T. J., and Cramer, L. P. (1996) *Cell* **84,** 371–379
3. Pollard, T. D., and Borisy, G. G. (2003) *Cell* **112,** 453–465
4. Brakebusch, C., and Fassler, R. (2003) *EMBO J.* **22,** 2324–2333
5. Blystone, S. D. (2004) *Biochim. Biophys. Acta* **1692,** 47–54
6. Pawlak, G., and Helfman, D. M. (2001) *Curr. Opin. Genet. Dev.* **11,** 41–47
7. Kahn, P., Heller, D., and Shin, S. (1983) *Cytogenet. Cell Genet.* **36,** 605–611
8. Labat-Robert, J. (2002) *Semin. Cancer Biol.* **12,** 187–195
9. Sadoul, R. (2006) *Biol. Cell* **98,** 69–77
10. Wu, Y., Pan, S., Luo, W., Lin, S. H., and Kuang, J. (2002) *Oncogene* **21,** 6801–6808
11. Wu, Y., Pan, S., Che, S., He, G., Nelman-Gonzalez, M., Weil, M. M., and Kuang, J. (2001) *Differentiation* **67,** 139–153
12. Vito, P., Pellegrini, L., Guiet, C., and D'Adamio, L. (1999) *J. Biol. Chem.* **274,** 1533–1540
13. Trioulier, Y., Torch, S., Blot, B., Cristina, N., Chatellard-Causse, C., Verna, J. M., and Sadoul, R. (2004) *J. Biol. Chem.* **279,** 2046–2052
14. Odorizzi, G., Katzmann, D. J., Babst, M., Audhya, A., and Emr, S. D. (2003) *J. Cell Sci.* **116,** 1893–1903
15. Luhtala, N., and Odorizzi, G. (2004) *J. Cell Biol.* **166,** 717–729
16. Matsuo, H., Chevallier, J., Mayran, N., Le Blanc, I., Ferguson, C., Faure, J., Blanc, N. S., Matile, S., Dubochet, J., Sadoul, R., Parton, R. G., Vilbois, F., and Gruenberg, J. (2004) *Science* **303,** 531–534
17. Kim, J., Sitaraman, S., Hierro, A., Beach, B. M., Odorizzi, G., and Hurley, J. H. (2005) *Dev. Cell* **8,** 937–947
18. Missotten, M., Nichols, A., Rieger, K., and Sadoul, R. (1999) *Cell Death Differ.* **6,** 124–129
19. Krebs, J., and Klemenz, R. (2000) *Biochim. Biophys. Acta* **1498,** 153–161
20. Shibata, H., Yamada, K., Mizuno, T., Yorikawa, C., Takahashi, H., Satoh, H., Kitaura, Y., and Maki, M. (2004) *J. Biochem.* (*Tokyo*) **135,** 117–128
21. Strack, B., Calistri, A., Craig, S., Popova, E., and Gottlinger, H. G. (2003) *Cell* **114,** 689–699
22. Katoh, K., Shibata, H., Suzuki, H., Nara, A., Ishidoh, K., Kominami, E., Yoshimori, T., and Maki, M. (2003) *J. Biol. Chem.* **278,** 39104–39113
23. von Schwedler, U. K., Stuchell, M., Muller, B., Ward, D. M., Chung, H. Y., Morita, E., Wang, H. E., Davis, T., He, G. P., Cimbora, D. M., Scott, A.,

Krausslich, H. G., Kaplan, J., Morham, S. G., and Sundquist, W. I. (2003) *Cell* **114,** 701–713
24. Schmidt, M. H., Chen, B., Randazzo, L. M., and Bogler, O. (2003) *J. Cell Sci.* **116,** 2845–2855
25. Elbashir, S. M., Harborth, J., Lendeckel, W., Yalcin, A., Weber, K., and Tuschl, T. (2001) *Nature* **411,** 494–498
26. He, G., Siddik, Z. H., Huang, Z., Khokhar, A. R., and Kuang, J. (2005) *Oncogene* **24,** 2929–2943
27. Yates-Siilata, K. E., Dahms, T. E., Webster, R. O., and Heuertz, R. M. (2004) *Cell Biol. Int.* **28,** 33–39
28. Banan, A., Zhang, Y., Losurdo, J., and Keshavarzian, A. (2000) *Gut* **46,** 830–837
29. Wulf, E., Deboben, A., Bautz, F. A., Faulstich, H., and Wieland, T. (1979) *Proc. Natl. Acad. Sci. U. S. A.* **76,** 4498–4502
30. Lengsfeld, A. M., Low, I., Wieland, T., Dancker, P., and Hasselbach, W. (1974) *Proc. Natl. Acad. Sci. U. S. A.* **71,** 2803–2807
31. Verderame, M., Alcorta, D., Egnor, M., Smith, K., and Pollack, R. (1980) *Proc. Natl. Acad. Sci. U. S. A.* **77,** 6624–6628
32. Carter, C. A., Doherty, M. M., Rusnak, D. W., Nettesheim, P., and Ferriola, P. C. (1994) *Exp. Cell Res.* **212,** 141–150
33. Bereiter-Hahn, J., and Kajstura, J. (1988) *Histochemistry* **90,** 271–276
34. Amankwah, K. S., and De Boni, U. (1994) *Exp. Cell Res.* **210,** 315–325
35. Jongstra-Bilen, J., Janmey, P. A., Hartwig, J. H., Galea, S., and Jongstra, J. (1992) *J. Cell Biol.* **118,** 1443–1453
36. Daly, R. J. (2004) *Biochem. J.* **382,** 13–25
37. Kinley, A. W., Weed, S. A., Weaver, A. M., Karginov, A. V., Bissonette, E., Cooper, J. A., and Parsons, J. T. (2003) *Curr. Biol.* **13,** 384–393
38. Cabezas, A., Bache, K. G., Brech, A., and Stenmark, H. (2005) *J. Cell Sci.* **118,** 2625–2635
39. Otey, C. A., and Carpen, O. (2004) *Cell Motil. Cytoskeleton* **58,** 104–111
40. Weaver, A. M., Young, M. E., Lee, W. L., and Cooper, J. A. (2003) *Curr. Opin. Cell Biol.* **15,** 23–30
41. Pollard, T. D., and Beltzner, C. C. (2002) *Curr. Opin. Struct. Biol.* **12,** 768–774
42. Higgs, H. N., and Pollard, T. D. (2001) *Annu. Rev. Biochem.* **70,** 649–676
43. Nickas, M. E., and Yaffe, M. P. (1996) *Mol. Cell. Biol.* **16,** 2585–2593
44. Kubler, E., and Riezman, H. (1993) *EMBO J.* **12,** 2855–2862
45. Chen, B., Borinstein, S. C., Gillis, J., Sykes, V. W., and Bogler, O. (2000) *J. Biol. Chem.* **275,** 19275–19281
46. Nakamura, K., Fujita, A., Murata, T., Watanabe, G., Mori, C., Fujita, J., Watanabe, N., Ishizaki, T., Yoshida, O., and Narumiya, S. (1999) *FEBS Lett.* **445,** 9–13
47. Peck, J. W., Oberst, M., Bouker, K. B., Bowden, E., and Burbelo, P. D. (2002) *J. Biol. Chem.* **277,** 43924–43932